Geochimica et Cosmochimica Acta 335 (2022) 98–110

Contents lists available at ScienceDirect

Geochimica et Cosmochimica Acta

journal homepage: www.elsevier.com/locate/gca

Experimental serpentinization of iron-rich olivine (hortonolite): Implications for hydrogen generation and secondary mineralization on Mars and icy moons

Thomas M. McCollom [a,*], Frieder Klein [b], Bruce Moskowitz [c,d], Peter Solheid [c,d]

[a] Laboratory for Atmospheric and Space Physics, University of Colorado, Boulder, CO 80309, USA
[b] Woods Hole Oceanographic Institution, Wood Hole, MA 02543, USA
[c] Department of Earth and Environmental Sciences, University of Minnesota, Minneapolis, MN 55455, USA
[d] Institute for Rock Magnetism, University of Minnesota, Minneapolis, MN 55455, USA

ARTICLE INFO

Article history:
Received 11 January 2022
Accepted 22 August 2022
Available online 28 August 2022
Associate editor: Gleb S. Pokrovski

Keywords:
Serpentinization
Experimental fluid-rock interactions
Thermodynamic models
Hydrothermal systems
Hydrogen
Mars
Icy moons
Astrobiology

ABSTRACT

Serpentinization of olivine-rich ultramafic rocks is recognized to have been widespread across the solar system throughout its history, with substantial implications for the chemical and physical properties of planetary lithospheres, atmospheric compositions, and astrobiology. One especially significant product of serpentinization is molecular hydrogen (H_2), whose generation is closely linked to the oxidation of Fe as serpentinization proceeds. While numerous experimental simulations of serpentinization have been conducted over the years, these studies have been performed almost exclusively using reactant minerals that contain relatively high Mg and low Fe contents representative of terrestrial mantle rocks. In contrast, very few studies have been conducted with the more Fe-enriched mineral compositions that may predominate on other solar system bodies. In this study, an experiment was conducted to investigate mineral alteration and H_2 generation during serpentinization of Fe-rich olivine (hortonolite; $Fo_{\sim 62}$) at 230 °C and 35 MPa. After 3500 h of reaction, ~55 % of the hortonolite reacted to secondary minerals composed of serpentine (chrysotile) and magnetite. Chrysotile contained proportionally less Fe than the original hortonolite, reflecting the partitioning of some Fe into magnetite; however, it contained substantially more Fe than serpentine precipitated from alteration of Mg-rich, Fe-poor terrestrial mantle olivine ($Fo_{\sim 90}$) under the same reaction conditions. Reaction of hortonolite also produced more than four times as much magnetite as Mg-rich olivine. Generation of H_2 occurred steadily throughout the experiment, with more than five times as much H_2 generated per mole of hortonolite reacted than observed for Fe-poor olivine at the same conditions. The results suggest that serpentinization of Fe-rich ultramafic rocks on Mars and other planetary bodies may have a substantially greater capacity to generate H_2 and to precipitate magnetite than their Fe-poor terrestrial counterparts, which would enhance their potential to support H_2-based biological communities, contribute to atmospheric warming, and augment local magnetic signatures in planetary lithospheres.

1. Introduction

Serpentinites are rocks that primarily form through the aqueous alteration of olivine-rich ultramafic rocks. For the most part, they form at low temperatures (<400 °C) in relatively shallow subsurface environments (Evans et al., 2013). Serpentinites have long been recognized to compose a significant fraction Earth's oceanic lithosphere (Cannat et al., 2010: Merdith et al., 2020), and are also prominent components of ophiolites and other subaerial terranes (Coleman, 1977). Over the last couple of decades, serpentinites have also gained increasing attention as components of the rocky mantles of Mars and of icy moons such as Enceladus and Europa (e.g., Vance et al., 2007, 2016; Milliken and Rivkin, 2009; Ehlmann et al., 2010; Michalski et al., 2013; Bultel et al., 2015; Hsu et al., 2015; Glein et al., 2015; Amador et al., 2018; Sekine et al., 2015; Waite et al., 2017; Vance and Melwani Daswani, 2020; Glein and Zolotov, 2020).

Much of the recent focus on serpentinites from planetary scientists is motivated by the observation that reduced volatile compounds, including molecular hydrogen (H_2) and methane (CH_4), are commonly generated in abundance as by-products of

* Corresponding author.
E-mail address: mccollom@lasp.colorado.edu (T.M. McCollom).

https://doi.org/10.1016/j.gca.2022.08.025
0016-7037/

the serpentinization process. On Earth, these compounds are recognized to support the growth of microbial communities in the absence of sunlight (Schrenk et al., 2013; McCollom and Seewald, 2013; Ménez, 2020) and can contribute to greenhouse warming of planetary atmospheres (Wordsworth and Pierrehumbert, 2013; Ramirez et al., 2014; Chassefière et al., 2016; Wordsworth et al., 2021). In addition, serpentinization can affect subduction dynamics and intraslab seismicity (e.g., Wada et al., 2008), and can result in precipitation of the mineral magnetite, which can make a significant contribution to magnetic signatures of planetary lithospheres (e.g., Toft et al., 1990; Quesnel et al., 2009; Klein et al., 2014; Lasue et al., 2015; Szitkar et al., 2017).

The process of serpentinization, and the production of H_2, CH_4, and magnetite that are formed as part of the process, has been the subject of numerous experimental and theoretical studies over the last several decades (e.g., Martin and Fyfe, 1970; Wegner and Ernst, 1983; Berndt et al., 1996; McCollom and Seewald, 2001; Seyfried et al., 2007; McCollom and Bach, 2009; Klein et al., 2009, 2013,2015; Jones et al., 2010; Marcaillou et al., 2011; Okamoto et al., 2011; Malvoisin et al., 2012; Shibuya et al., 2015; Grozeva et al., 2017; McCollom et al., 2016, 2020a,b). These studies, however, have focused almost exclusively on serpentinization of the Mg-rich ultramafic rocks that dominate the terrestrial mantle. In contrast, few studies have examined serpentinization of more Fe-rich rock compositions like those that may occur in the lithospheres of Mars, icy moons, and other planetary bodies (e.g., Moody, 1976; Tutolo et al., 2019; McCollom et al., 2022).

Serpentinization is commonly represented by the simplified reaction:

$$\text{Olivine} + H_2O \rightarrow \text{Serpentine} \pm \text{Brucite} \pm \text{Magnetite} + H_2 \quad (1)$$

However, this simple reaction does not accurately reflect the substantial variability in product minerals and their chemical compositions that can occur under different circumstances. Serpentinization of olivine can be represented in somewhat more comprehensive terms by the reaction:

$$\begin{aligned}&(Mg,Fe)_2SiO_4[\text{olivine}] + vH_2O \rightarrow w\left(Mg,Fe^{II},Fe^{III}\right)_3\left(Si,Fe^{III}\right)_2\\&O_5(OH)_4[\text{serpentine}] \pm x\left(Mg,Fe^{II}\right)(OH)_2\,[\text{brucite}]\\&\pm yFe^{II}Fe^{III}_2O_4\,[\text{magnetite}] + zH_2\end{aligned} \quad (2)$$

which reflects the extensive solid-solution mixing that occurs in olivine and the product minerals serpentine and brucite. The stoichiometry of the reaction, as reflected in the coefficients v-z, and the compositions of individual product minerals can be highly variable depending on reaction conditions and reactant mineral compositions (e.g., McCollom and Bach, 2009; Klein et al., 2009, 2013; McCollom et al., 2016, 2022). Production of H_2 during the reaction is coupled to the oxidation of ferrous Fe (Fe^{II}) to ferric Fe (Fe^{III}), which can be expressed in general as:

$$2[Fe^{II}O] + H_2O \rightarrow [Fe^{III}_2O_3] + H_2 \quad (3)$$

where $[Fe^{II}O]$ and $[Fe^{III}_2O_3]$ represent components of olivine and secondary minerals, respectively. The H_2 generated can potentially react with CO_2 to form CH_4 and other organic compounds through reactions such as:

$$CO_2 + 4H_2 \rightarrow CH_4 + H_2O \quad (4)$$

(e.g., Proskurowksi et al., 2008; Klein et al., 2019), although kinetic inhibitions may prevent such reactions from proceeding under many circumstances (McCollom and Seewald, 2007; McCollom, 2013, 2016).

The ultramafic rocks that are the precursors for most terrestrial serpentinites contain minerals with relatively Mg-rich compositions, which is evidently the result of partitioning of large amounts of Fe into Earth's core (Agee, 1993). For example, the mantle-derived peridotites that are the most common precursor of terrestrial serpentinites contain forsteritic olivine with compositions around Mg# = 90 [where Mg# = Mg/(Mg + Fe) on a molar basis]. In contrast, the olivine that may serve as the precursor for serpentine minerals on other planetary bodies may have compositions that are substantially more enriched in Fe. For example, olivine in most martian rocks has high Fe contents relative to the terrestrial mantle, with typical Mg# values in the 50–70 range (Koeppen and Hamilton, 2008; Papike et al., 2009; Hicks et al., 2014), and the martian mantle is thought to be substantially enriched in Fe relative to Earth's (Khan and Connolly, 2008; Yoshizaki and McDonough, 2020). Olivine in meteorites have widely variable Fe contents, but in many instances they also have substantially higher Fe contents than those of terrestrial mantle rocks (e.g., McSween, 1977; Rubin, 1990; Keller and Buseck, 1990; Hanowski and Brearley, 2001; Velbel et al., 2012, 2015). The compositions of rocks in the interiors of icy moons are unknown but, depending on the extent of core formation and other factors, they may also have mineral compositions that are substantially more Fe-rich than terrestrial mantle rocks, similar to the interior of Mars (e.g., Vance and Melwani Daswani, 2020).

It is to be expected that serpentinization of Fe-rich olivine should result in secondary mineral products that have higher Fe contents and, thus, generate greater amounts of H_2 than would occur during reaction of Fe-poor olivine. However, it is not immediately evident how the higher Fe contents will be distributed among the mineral products of serpentinization, or how much production of H_2 will increase as a function of olivine Fe content. It has been observed, for instance, that the Fe content of serpentine minerals across individual meteorites is nearly uniform regardless of the Fe content of adjacent olivine crystals (e.g., Hanowski and Brearley, 2001; Velbel et al., 2012, 2015). This observation might indicate that the amount of Fe partitioned into serpentine is largely independent of the initial olivine composition, resulting in a proportional increase in the amount of Fe that precipitates in other reaction products. Alternatively, geochemical models that assume thermodynamic equilibrium among the products of serpentinization predict that the Fe content of serpentine should increase steadily with increasingly higher Fe contents in olivine (Klein et al., 2013; McCollom et al., 2022). These models also predict generally increasing H_2 production as well as increased amounts of Fe in brucite and magnetite for higher Fe contents in olivine, but the relative abundances of these products are also predicted to be strongly dependent on reaction temperature. If valid, the thermodynamic model predictions suggest that serpentinization of ultramafic rocks on other planetary bodies may have a substantially greater capacity to support H_2-based biological activities, enhance greenhouse warming, and effect the magnetic properties of lithospheres.

The accuracy of the thermodynamic model predictions, however, remains untested for Fe-rich olivine compositions. Moreover, it remains uncertain whether thermodynamic equilibrium or some other factor exerts the predominant control on mineral composition and H_2 generation during serpentinization. Over the years, various different environmental factors have been proposed to exert a strong influence on the relative abundance and chemical composition of secondary minerals during serpentinization, including factors such as the prevailing activity of silica, the evolving oxidation state of the system, fluid pH, reaction kinetics, attainment of thermodynamic equilibrium between the reacting olivine and resulting serpentine, and thermodynamic equilibrium among the reaction products including minerals and dissolved species (e.g., Moody, 1976; Evans and Trommsdorf, 1972; Frost and Beard, 2007; Seyfried et al., 2007; Evans, 2008; McCollom and Bach, 2009; McCollom et al., 2016, 2020a,2022; Syverson et al., 2017; Mayhew and Ellison, 2020). Thus, experimental study is

needed to further assess the accuracy of thermodynamic models and determine their applicability to serpentinization of Fe-rich ultramafic rocks.

Accordingly, a laboratory experiment was conducted to investigate serpentinization of an Fe-rich olivine variety, hortonolite (Mg# = 62). The conditions and methods used in the experiment were designed to parallel those employed in a previous set of experiments performed with relatively Fe-poor, Mg-rich terrestrial mantle olivine (Mg# = 90; McCollom et al., 2016, 2020a). The parallel reaction conditions allow for direct comparisons among experimental results in order to examine the effect of Fe content on reaction products, including both fluid chemistry and secondary minerals. The study focused in particular on the impact of the higher Fe contents on H_2 generation and partitioning of Fe among the product minerals. The results show enhanced production of H_2 and magnetite from hortonolite relative to more Mg-rich olivine compositions, consistent with thermodynamic predictions (Klein et al., 2013; McCollom et al., 2022).

2. Methods

The laboratory experiment (designated Hortono230) was conducted by heating finely powdered hortonolite with a solution initially containing 485 mmol kg^{-1} NaCl. The experiment consisted of 8.3 g hortonolite and 48.3 g fluid, and was heated for 3500 h (146 d) at 230 °C and 35 MPa. The reaction conditions were nominally selected to represent serpentinization in the shallow subsurface of a planetary body. On Earth, serpentinization takes place over a wide range of temperatures from < 100 °C to > 400 °C (e.g., Evans et al., 2013; Klein et al., 2014; Templeton et al., 2021). However, the upper temperature limit for serpentinization of olivine decreases with increasing Fe content (McCollom et al., 2022), which restricted the possible temperature range to <300 °C at the experimental pressure. The reaction temperature of 230 °C was selected for Hortono230 as an intermediate between the upper limit and lower temperatures where reactions would be too slow to observe substantial reaction on laboratory timescales. In addition, performing the experiment at 230 °C allows for direct comparison with a suite of previous experiments performed with Mg-rich olivine at this temperature using the same methodology (McCollom et al., 2016; 2020a, 2020b). The reaction temperature of 230 °C is also close to the temperature thought to prevail in the subsurface reaction zone of the Lost City deep-sea hydrothermal system, a well-studied site of serpentinization on Earth (Proskurowksi et al., 2006; Foustoukos et al., 2008).

Production of dissolved H_2 and other changes in fluid composition were monitored at intervals throughout the experiment. Solids were recovered at the end of the experiment and analyzed for their mineralogy and chemical composition. Methods used to prepare the reactants and to analyze the fluids and solid reaction products are summarized below, with additional details provided as supplemental materials.

The experiment was conducted in a flexible-cell hydrothermal apparatus using a gold reaction cell with titanium fittings (Supplemental Fig. S1; Seyfried et al., 1987). The reaction cell was contained within a stainless steel pressure housing, with water used as the external pressurizing medium. An external valve connected to the reaction cell with a capillary tube allowed fluids to be sampled and analyzed during the experiment. The flexibility of the gold reaction cell allowed fluids to be sampled at experimental conditions, and also eliminated the presence of a vapor headspace so that reactions were confined to the aqueous phase. The titanium fittings were heated in air for >24 h at 450 °C prior to use in order to form a relatively inert TiO_2 surface layer.

The experiment used hortonolite extracted from a hortonolite dunite from the type locality at the O'Neil Mine in Monroe, Orange County, NY. The dunite was predominantly composed of hortonolite, but also contained minor impurities that included magnetite, Cr-rich spinel (Cr-spinel), ilmenite, chalcopyrite, amphibole (actinolite-tremolite), diopside, orthopyroxene, and serpentine (Fe-rich lizardite). The hortonolite has an average composition of $Mg_{1.24}Fe_{0.76}SiO_4$, which equates to Mg# = 62 or, equivalently, Fo_{62} when expressed on the percent forsterite endmember scale (Table 1).

Extensive efforts were made to purify the hortonolite as much as possible prior to the experiment, employing a combination of hand picking under a microscope and repeated separation using a sodium polytungstate high-density liquid (GeoLiquids, Prospect Heights, IL) and a magnetic separator (Frantz, Tullytown, PA). Despite these efforts, the materials used in the experiment con-

Table 1
Chemical compositions of starting minerals and reaction products determined by EMPA.

Oxide (wt.%)	Hortonolite (n = 16)	Opx† (n = 1)	Cpx† (n = 2)	Cr-spinel† (n = 3)	Hortono230 Chrysotile (n = 11)	Hortono230 Magnetite (n = 4)
SiO_2	36.3 (1.0)	54.7	52.6	0.03	32.4 (1.7)	6.1
TiO_2	b.d.	0.08	0.23	2.3	b.d.	0.08
Al_2O_3	b.d.	0.43	1.1	9.5	b.d.	b.d.
Cr_2O_3	b.d.	0.13	0.29	41.2	b.d.	0.74
FeO#	32.8 (1.9)	18.0	7.2	38.7	10.5 (0.8)	27.4
Fe_2O_3	–	–	–	–	–	60.8
MgO	29.5 (1.8)	25.6	15.0	2.0	26.3 (1.8)	0.67
MnO	0.48 (0.05)	0.43	0.21	0.47	0.37 (0.05)	0.50
CaO	0.06 (0.01)	1.05	21.6	b.d.	0.08 (0.02)	0.29
Na_2O	b.d.	b.d.	0.26	b.d.	0.10 (0.14)	b.d.
K_2O	b.d.	b.d.	b.d.	b.d.	b.d.	b.d.
NiO	0.39 (0.04)	0.06	0.07	0.15	0.32 (0.12)	0.30
CoO	b.d.	b.d.	b.d.	b.d.	b.d.	–
Cl	b.d.	b.d.	b.d.	b.d.	0.42 (0.23)	b.d.
Total	99.6 (1.4)	100.5	98.6	94	71 (4)	96.8
Mg#	62 (3)	72	79	–	82 (1)	–
(Mg + Fe):Si*	1.97	0.97	0.54	–	1.48	–

Data for reaction products are average values (n = number of analyses) with standard deviation in parentheses where appropriate. b.d. = below detection of approximately 0.1 wt%.
*Molar ratio.
Total Fe reported as FeO except for magnetite.
† Present as trace components in hortonolite reactant. "–" = no data.

tained small amounts of contaminating phases (<2 vol% based on point counts of images of the prepared reactant obtained using scanning electron microscopy coupled with electron dispersive X-ray spectroscopy). The contaminants were predominantly Cr-spinel and clinopyroxene (Cpx) along with trace amounts of orthopyroxene (Opx). The chemical compositions of the contaminating minerals are included in Table 1.

Following separation, the minerals were washed in acetone and then sonicated several times in deionized water (18.2 Ω). Prior to the experiment, the separated minerals were pulverized in an agate mortar and pestle, and sieved to obtain a fine powder (<53 μm). The small grain size was utilized in order to promote a significant degree of reaction on a reasonable time scale as well as to allow direct comparison with other serpentinization experiments conducted at the same temperature that also utilized finely powdered starting materials (McCollom et al., 2016, 2020a).

At intervals throughout the experiment, several fluid aliquots (0.3–1 g each) were obtained through the sample valve directly into gas-tight glass syringes and analyzed for the abundance of: (1) dissolved H_2, (2) total dissolved CO_2 ($\Sigma CO_2 = CO_{2(aq)} + HCO_3^- + CO_3^{2-}$), CH_4, and C_2-C_6 hydrocarbons, (3) room temperature pH ($pH_{25°C}$), and (4) dissolved rock-forming elements. Analytical methods followed those described previously (McCollom et al., 2016, 2020a). Briefly, volatile compounds were analyzed by gas chromatography (GC) using a combination of thermoconductivity detection (TCD) and Flame Ionization Detection (FID), with estimated analytical errors ± 5 %. The $pH_{25°C}$ was measured using a Ross micro combination electrode at room temperature with an uncertainty of approximately ± 0.1 units of the reported value. Dissolved SiO_2 was measured by photospectrometry immediately after sampling, while total dissolved Na, Ca, Mg, Fe, Al, and K were analyzed by Inductively Coupled Plasma – Optical Emission Spectroscopy (ICP-OES) on a fluid aliquot acidified with HNO_3.

At the termination of the experiment, the solids were removed, filtered, and rinsed several times with ethanol in an effort to remove any remaining experimental fluid that might leave behind salt deposits when dried. Several methods were employed to characterize the solid products, including scanning electron microscopy coupled with electron dispersive X-ray spectroscopy (SEM/EDS), electron microprobe analysis (EMPA), X-ray diffraction (XRD), confocal Raman spectroscopy, thermogravimetric analysis (TGA), Mössbauer spectroscopy (MS), magnetization, and visible-near infrared spectroscopy (VNIR). Details of the analytical methods are provided in the Supplemental Materials.

Reaction path models and fluid speciation calculations were utilized to aid in the interpretation of the experimental data. The models were performed with the software package EQ3/6, version 8.0a (Wolery and Jarek, 2003). The thermodynamic database used for the calculations is described in McCollom and Bach (2009) and Klein et al. (2013), and is the same as that used by McCollom et al. (2022). The database was constructed for a constant pressure of 35 MPa and includes solid solution models for a number of minerals including serpentine and brucite. Most solid solutions assume ideal mixing; however, the serpentine solid solution assumes ideal mixing with a site parameter of 2.5 with three endmembers (chrysotile, greenalite, and cronstedtite) (Klein et al., 2013) to account for mixing on two sites and incorporation of both Fe^{II} and Fe^{III}. An ideal mixing model was used for olivine with two endmembers (forsterite and fayalite) and a site parameter equal to two to reflect mixing of Mg and Fe on two sites. The thermodynamic database used in the calculations is provided as supplemental materials (Dataset1).

Fluid speciation calculations were performed to estimate in situ pH, utilizing the program EQ3. The calculations were performed in two steps. First, the fluid was speciated at 25 °C using the measured fluid compositions and room temperature pH, adjusting for charge balance with Cl. The adjusted Cl abundance from the 25 °C calculation was then used with other measured concentrations to respeciate the fluid at 230 °C, with charge balance on H^+ determining the in situ pH.

Reaction path models were constructed using EQ6 to simulate serpentinization of hortonolite for comparison with the experimental results, using methods similar to those employed by McCollom et al. (2020b, 2022). The reaction path model simulates incremental dissolution of hortonolite and equilibrium precipitation of secondary minerals from the solution (Bethke, 2008). The output of the model is a prediction of the evolving compositions of secondary minerals and the co-existing fluid as the reaction proceeds, assuming thermodynamic equilibrium is maintained among the fluid and solid products. At the conditions of the experiment, olivine is thermodynamically unstable relative to the products of serpentinization (e.g., Klein et al., 2013; McCollom et al., 2022); consequently, it reacts irreversibly and cannot equilibrate with the reaction products. The model was constructed using the same starting mineral and fluid compositions as the experiment, and with the same water:rock ratio.

3. Results

3.1. Fluid chemistry

Measured fluid compositions during Hortono230 are listed in Table 2, and the evolution of selected fluid components during the experiment are displayed in Fig. 1. Also shown in Fig. 1 for comparison are results from two other olivine serpentinization experiments that were performed with Mg-rich olivine as the mineral reactant rather than hortonolite (i.e., Oliv230fine and Oliv230pH; McCollom et al., 2016, 2020a). The olivine used in these other experiments is derived from mantle xenoliths (San Carlos, AZ, USA) and has a Mg# ≈ 90 (referred to here as SC olivine).

Table 2
Fluid compositions during experiment Hortono230.

Time (*h*)	Temp (°C)	H_2 (*m*)	CO_2 (*m*)	CH_4 (*μ*)	Na (*m*)	Cl (*m*)	Si (*μ*)	Fe (*μ*)	Mg (*μ*)	Ca (*μ*)	Al (*μ*)	K (*μ*)	pH 25 °C	pH in situ	H_2 gen.[#] (*μmol/g*)	Fluid[†] (*g*)
0	230	*Start of experiment*														
21	230	0.31	0.44	5.2	470	–	210	56	110	120	b.d.	130	7.1	5.7	7.8	48.6
742	230	24.6	–	–	460	–	51	58	b.d.	120	b.d.	130	10.0	7.8	129	43.6
1580	230	60.0	–	–	383	–	53	61	b.d.	120	b.d.	130	10.3	7.4	197	39.4
2372	230	79.3	0.14		450	–	41	150	b.d.	130	b.d.	130	10.3	7.4	381	35.9
3500	230	88.5	0.10		450	–	41	70	80	120	b.d.	130	10.3	7.4	417	32.3
3525	25	*Cooled to room temperature*														
3526	25	–	–	–	440	–	34	25	44	120	b.d.	130	–	–	–	25.0

Concentrations in mmol kg^{-1} (*m*) or μmol kg^{-1} (*μ*). "–" = not measured.
[#] Hydrogen generated per gram of reactant hortonolite.
[†] Amount of fluid in reaction cell at time of sampling.

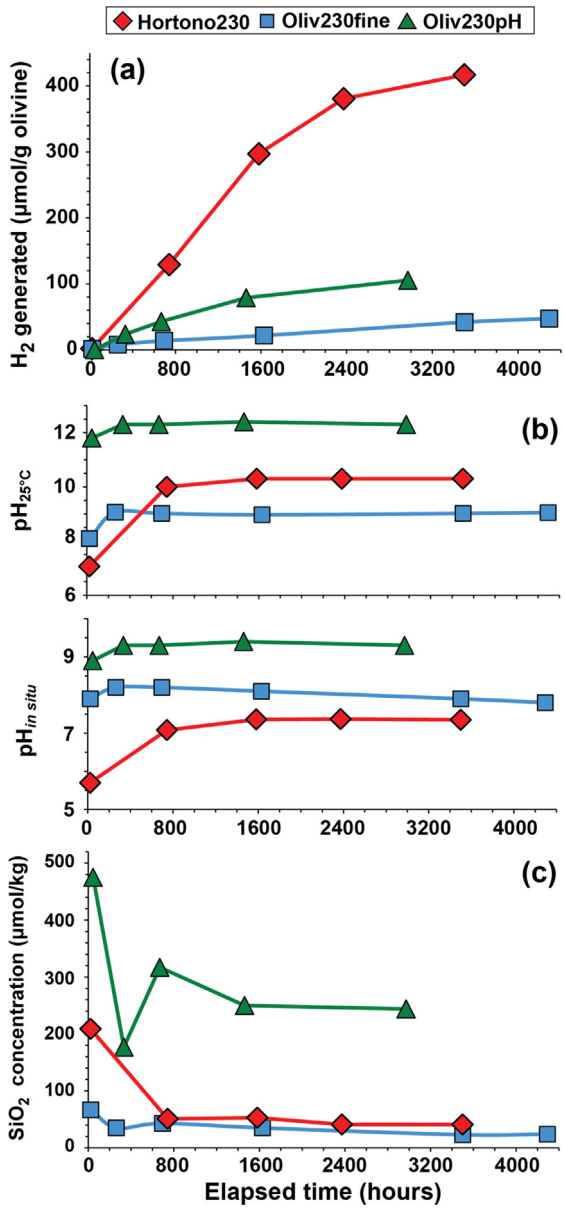

Fig. 1. Fluid composition during Hortono230, with results of two other serpentinization experiments performed at similar conditions but using Mg-rich olivine (Mg# = 90) shown for comparison (Oliv230fine and Oliv230pH; McCollom et al., 2016, 2020a). (a) Total amount of H_2 generated per g of reactant olivine. (b) Measured room temperature pH ($pH_{25°C}$) and calculated in situ pH ($pH_{in\ situ}$). (c) Dissolved ΣSiO_2 concentration.

Both of these other experiments were conducted at the same temperature (230 °C) and used the same grain size (<53 μm) as Hortono230, and were performed with the same experimental procedures. However, the initial reactant fluid for Oliv230fine contained 20 mmol kg^{-1} $NaHCO_3$ in addition to NaCl, while the fluid for Oliv230pH was augmented with 38 mmol kg^{-1} NaOH in order to raise the pH of the experiment and the $NaHCO_3$ concentration was reduced to 3 mmol kg^{-1}.

As seen in Fig. 1a, production of H_2 commenced immediately after initiation of heating of Hortono230 and continued throughout the experiment. The rate of H_2 production appeared to be constant during the first ~1600 h of the experiment, but it tapered off slightly at the last measurement. Throughout Hortono230, H_2 production was substantially higher than either of the Mg-rich olivine experiments performed under similar conditions (Fig. 1a). Note that the amounts of H_2 in the figure are expressed in terms of μmoles generated per g reactant olivine in order to account for differences in the relative amounts of olivine and fluid used in the experiments.

The room-temperature pH ($pH_{25°C}$) of the fluid was circumneutral at the beginning of Hortono230, but increased to moderately alkaline conditions ($pH_{25°C} \approx 10$) by the time of the second sample at 742 h (Fig. 1b). The $pH_{25°C}$ then remained essentially constant for the remainder of the experiment. The calculated in situ pH ($pH_{in\ situ}$) of Hortono230 was moderately alkaline with values around 7.4 throughout most of the experiment (Fig. 1b; neutral pH at the experimental conditions is ~5.5). The concentration of total dissolved silica (ΣSiO_2) rose to 210 μmol kg^{-1} at the first sample, but then decreased and remained essentially constant at 40–53 μmol kg^{-1} for the remainder of the experiment (Fig. 1c). The ΣSiO_2 concentration during most of Hortono230 was very similar to that in Oliv230fine, but substantially lower than that observed in Oliv230pH. The higher ΣSiO_2 concentration in Oliv230pH is largely attributable to increased abundance of $HSiO_3^-$ at the higher pH of the experiment (McCollom et al., 2020a). Most dissolved cations (Fe, Ca, K, and Mg) maintained essentially steady concentrations throughout the experiment at levels between 60 and 130 μmol kg^{-1}, while Al was below detection (Table 2).

3.2. Solid products

Inspection of the solids by SEM following the experiment identified only serpentine and magnetite as reaction products (Fig. 2), and these were also the only products identified by XRD (Supplemental Figure S2). The serpentine has a fibrous texture consistent with chrysotile (Fig. 2a), and the Raman spectrum is also indicative of chrysotile (Supplemental Figure S3). The chrysotile has an Mg# = 82 (Table 1), indicating it is depleted in Fe relative to the original hortonolite (Mg# = 62). Magnetite contains several wt.% SiO_2 (Table 1). Some of this SiO_2 may be accounted for by chrysotile fibers intergrown with the magnetite, but the low Mg content indicates that a significant amount of SiO_2 may be incorporated into the magnetite structure. Minor cation substitution in the magnetite is consistent with a slight lowering of the observed Curie temperature (T_C = 779 K) from its value for pure magnetite (T_C = 848 K) and the absence of the Verwey transition for magnetite at 120 K (Supplemental Figure S4).

In addition to serpentine and magnetite, the reacted solids also contained substantial amounts of unreacted hortonolite and small amounts of Cr-spinel (Fig. 2). The Cr-spinel showed no evidence that it reacted during the experiment. In some cases, remnant Cr-spinel crystals were surrounded by a layer of magnetite, but the absence of Cr and Al in the magnetite layer indicated that it had precipitated directly from solution rather than forming as an alteration product of the Cr-spinel (Supplemental Fig. S5). Furthermore, small amounts of Cr and Al might be expected to occur in serpentine if some Cr-spinel had dissolved (Andreani et al., 2013); however, these elements were below detection (<0.1 wt%) in the chrysotile from Hortono230, even in the immediate vicinity of relict Cr-spinel. Scattered crystals of relict Cpx were also observed among the solids and showed little apparent evidence of reaction, while no remaining Opx was found.

Two distinct zones were evident in the solid reaction products, one of which was dark grey in tone and the other light grey. The dark grey toned material comprised the predominant fraction of the bulk products (~80 vol%). Inspection of the zones by SEM indicated that the light grey zones contained fewer and smaller remnant olivine crystals than the dark grey areas (Fig. 2). Magnetization measurements indicated that the light grey zones contain a somewhat higher weight fraction of magnetite (19.8 wt

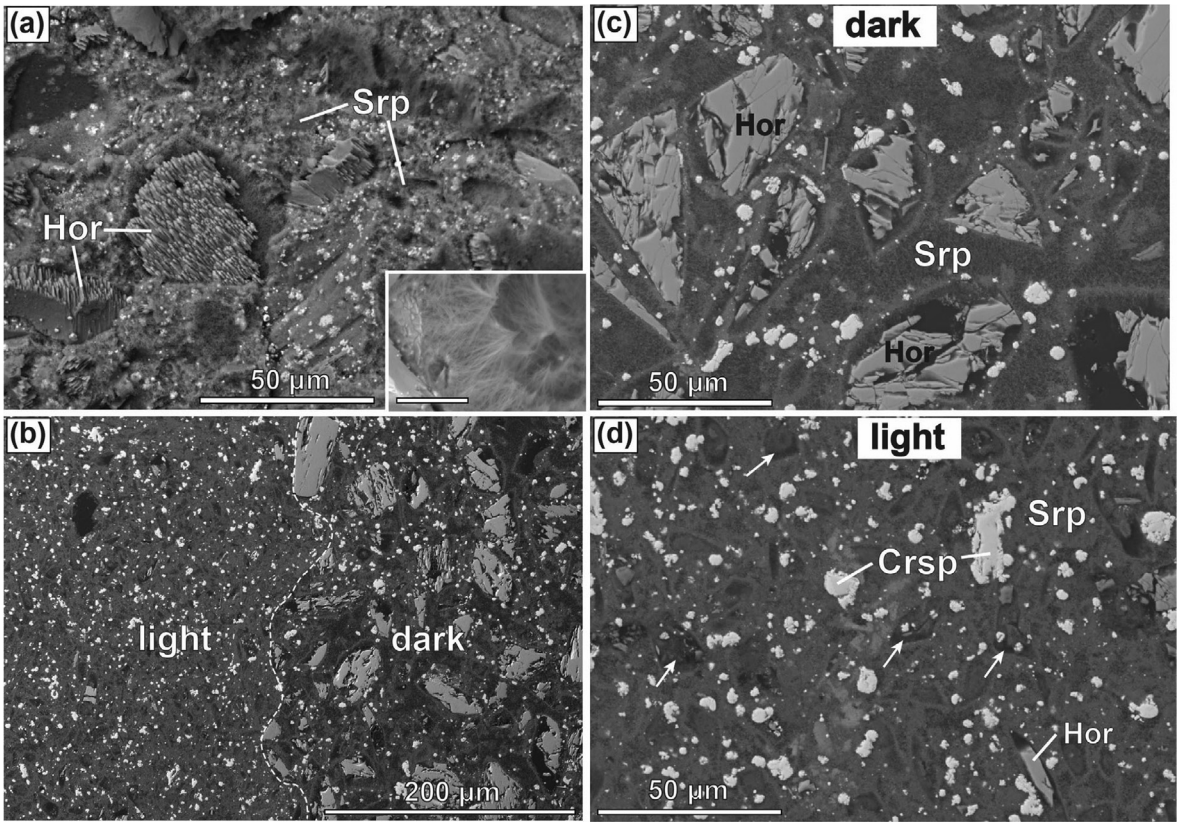

Fig. 2. Back-scattered electron (BSE) images of reaction products from Hortono230. (a) Grain mount showing relict hortonolite (Hor) embedded in a dense mat of chrysotile serpentine fibers (Srp) and magnetite (bright spots). The dentate features on the surfaces of the hortonolite are typical for olivine dissolution (e.g., Velbel, 2009; Malvoisin et al., 2012; McCollom et al., 2016). The inset shows a magnified view of chrysotile fibers (scale bar is 30 µm). (b) Image of polished thin section illustrating the differences in mineral distribution between light- and dark-grey toned zones in the bulk solid products, with the dashed white line marking the sharp boundary between the zones. (c,d) Enlarged views of light- and dark-toned zones. In (d), there are many small crystal-shaped regions outlined by accumulations of chrysotile, a few of which are identified by white arrows. These are probably voids left behind by the removal of small hortonolite crystals during polishing. Except for the large Cr-spinel crystals (Crsp) identified in (d), virtually all bright minerals in images are magnetite.

%) than the dark zones (14.7 wt%; average of two measurements for each zone). Chemical analyses of the serpentine and magnetite by EMPA did not reveal any differences in the chemical compositions for the secondary minerals in the two zones. The presence of these distinct zones contrasts with other olivine serpentinization experiments conducted using the same methods, where the products have typically been found to be highly homogenous throughout the sample (e.g., McCollom et al., 2016, 2020a). The cause of the zonation is undetermined at this time.

Thermogravimetric analysis of the reacted solids exhibited weight loss only for chrysotile (Fig. 3). The total loss attributable to decomposition of chrysotile is 4.8 wt% in the darker-toned solids and 6.0 wt% for the lighter-toned solids (Table 3). When combined with the amount of magnetite produced, these weight losses equate to approximately 52 % and 67 % hortonolite reaction for the dark and light zones, respectively, since OH constitutes ~12 wt% of serpentine for Mg# = 82 (Table 3). Based on the estimate that the darker materials comprise ~80 % of the bulk solids, these results indicate approximately 55 % of the original hortonolite reacted during the experiment.

To obtain additional information on the partitioning of Fe among secondary phases, Mössbauer spectroscopy (MB) was performed on the reaction products (Supplemental Figure S6). In order to focus on the state of Fe in chrysotile, the analysis was performed on materials that had been processed to remove magnetite and increase the chrysotile:hortonolite ratio. During this process, the reacted solids were lightly crushed, combined with ethanol in a glass vial, and sonicated. The suspended fraction was then removed with a pipette and evaporated, and the residue was retained for the MB analysis. A strong magnet placed next to the glass vial during removal of the ethanol excluded magnetite from the suspended fraction.

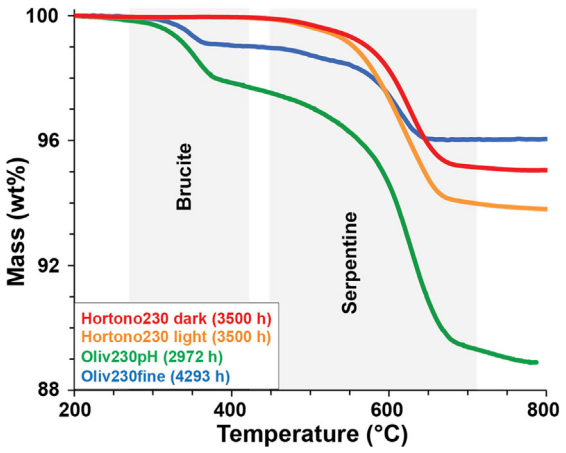

Fig. 3. Results of thermogravimetric analysis of reacted solids from Hortono230, with results of two experiments performed at similar conditions using SC olivine (Mg# = 90) shown for comparison (Oliv230fine, Oliv230pH; McCollom et al., 2016, 2020a). Mass loss between 270 °C and 430 °C is attributed to brucite, while that between 450 and 730 °C is attributed to chrysotile serpentine (Viti, 2010). Separate measurements were made on the dark-grey and light-grey zones in the Hortono230 products.

Table 3
Results of thermogravimetric analyses and magnetization measurements.

	Hortono230 Dark	Hortono230 Light	Oliv230fine*	Oliv230pH*
TGA weight loss (%):				
Serpentine	4.8	6.0	3.0	8.1
Brucite	0	0	0.9	2.3
Secondary minerals (wt.%):				
Serpentine	39	49	23	64
Brucite	0	0	3.0	7.6
Magnetite#	15	20	1.75	1.6
Total reaction (%)†	52	67	25	69
Duration (h)	3500	3500	4293	2972

* Results from McCollom et al. (2016, 2020a).
\# From magnetization measurements.
† Estimated percent of total primary minerals reacted, by mass. See Supplemental Materials for details of the calculation.

Mössbauer parameters for the processed sample are summarized in Table 4 and displayed in Fig. 4. Also shown in Fig. 4 are MB parameters for reference minerals and for serpentine from several previous olivine serpentinization experiments. The MB results indicate that both Fe^{II} and Fe^{III} are present in the chrysotile, with an Fe^{III}:Fe_{total} ratio of about 21 % (calculated by dividing the total amount of Fe^{III} present in both octahedral and tetrahedral sites by the total amount in chrysotile; Table 4). Of the Fe^{III}, approximately-two-thirds resides in octahedral sites, while one-third resides in tetrahedral sites.

Because remote spectroscopy is commonly used to investigate minerals on the surfaces of other planetary bodies, visible-near infrared (VNIR) reflectance spectra were collected for the products of Hortono230 and other olivine serpentinization experiments (Fig. 5). The experimental products all display prominent absorption features at ~1.39, ~1.93, and ~2.33 μm that are consistent with chrysotile. In addition, the features at ~1.39 μm and ~2.33 μm data appear to show a slight increase in wavelength with increasing Fe contents (i.e., lower Mg#).

4. Discussion

4.1. Partitioning of Fe and H_2 generation

Key results from the Hortono230 experiment are summarized in Table 5, together with results from comparable experiments performed using Mg-rich SC olivine. As illustrated in Fig. 1a, reaction of hortonolite generated substantially greater amounts of H_2 per gram than was observed during serpentinization of Mg-rich olivine. When differences in extent of reaction are taken into account, serpentinization of hortonolite produced approximately 4–5 times as much H_2 per gram as Mg-rich olivine under comparable conditions (Table 5). Similarly, the amount of magnetite precipitated from reaction of hortonolite was 4–12 times greater than that observed for Mg-rich olivine, once the differing extents of reaction are taken into account (Table 5). In addition, serpentine from Hortono230 is substantially enriched in Fe (Mg# = 82) relative to that produced during experimental serpentinization of Mg-rich olivine, which typically has compositions of Mg# = 92–97 for comparable reaction conditions (Okamoto et al., 2011; Malvoisin et al., 2012; Ogasawara et al., 2013; McCollom et al.,

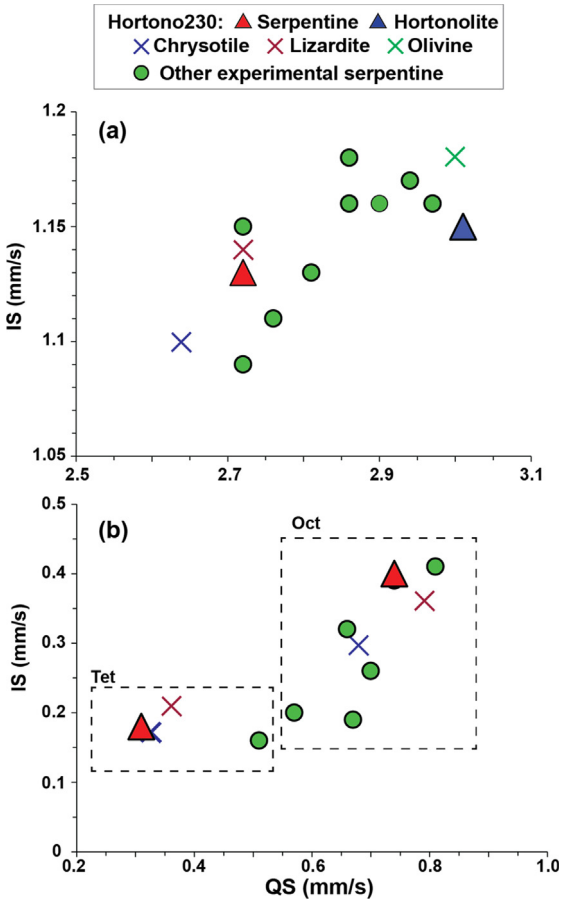

Fig. 4. Isomer shift (IS) versus quadrupole splitting (QS) from Mössbauer analysis of serpentine produced in Hortono230 (red triangles) along with data for the original hortonolite (blue triangle). Also shown are data for several relevant reference minerals (crosses; from Dyar et al., 2006) and for serpentine produced during other olivine serpentinization experiments (green circles; McCollom et al., 2016, 2020a). (a) Parameters attributable to Fe^{II}. (b) Parameters attributable to Fe^{III}. Dashed boxes in (b) outline parameters assigned to tetrahedral (Tet) or octahedral (Oct) sites for serpentine minerals. The Mössbauer measurements were performed on reacted solids that had been processed to remove magnetite and enhance the serpentine: hortonolite ratio (see Supplemental Methods). The measured MB spectra and fit curves for Hortono230 are shown in Supplemental Fig. S6. (For interpretation of the references to colour in this figure legend, the reader is referred to the web version of this article.)

Table 4
Room-temperature hyperfine magnetic Mössbauer parameters for reaction products from Hortono230 that were processed to remove magnetite and some hortonolite.

QS (mm/s)	IS (mm/s)	%*	Assignment
2.72	1.13	69	Fe^{II} (serp)
0.74	0.40	12	Fe^{III} (serp; oct)
0.31	0.18	6	Fe^{III} (serp; tet)
3.01	1.15	13	Fe^{II} (hor)

* Relative molar abundances of Fe among the components. Peak assignments for Fe^{III} include both octahedral (oct) and tetrahedral (tet) sites. Mineral abbreviations: serp = chrysotile serpentine, hor = hortonolite.

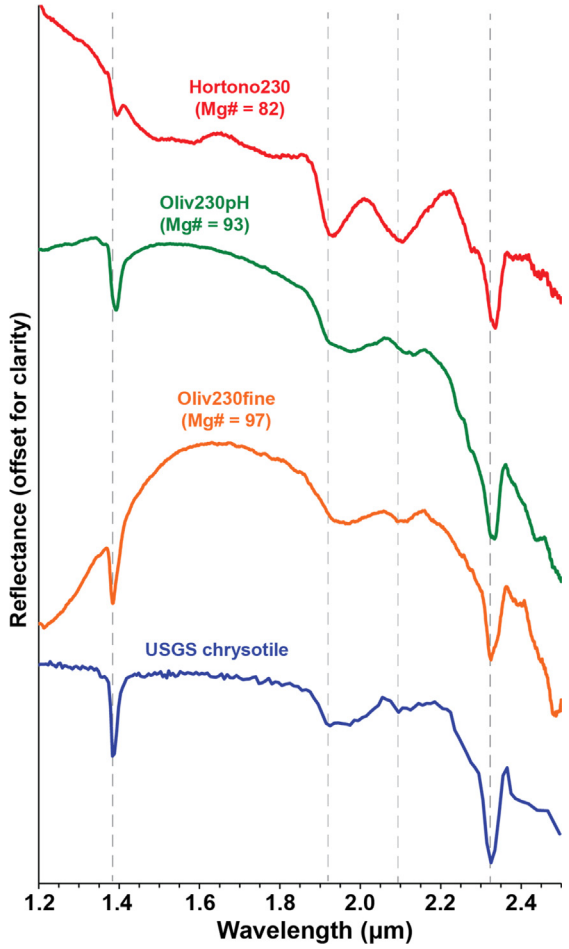

Fig. 5. Visible/near-infrared reflectance spectrum of serpentine from the Hortono230 experiment compared with spectra for other olivine serpentinization experiments and with a USGS reference spectrum for chrysotile (Kokaly et al., 2017). No compositional data is available for the USGS reference sample.

2016, 2020a). Furthermore, brucite was absent from the secondary mineral products of Hortono230 whereas it was produced in substantial amounts during reaction of Fe-poor SC olivine under the same conditions (McCollom et al., 2016, 2020a).

All of these results are consistent with predictions of thermodynamic equilibrium models for serpentinization of olivine with variable Fe contents (Klein et al., 2013; McCollom et al., 2022). The models predict that serpentinization of olivine with increasingly higher Fe contents should result in precipitation of greater amounts of magnetite, the formation of serpentine minerals with higher Fe contents, and generation of greater amounts of H_2 from each increment of olivine reacted. At 230 °C, equilibrium models also predict that reaction of olivine with high Fe contents should not precipitate any brucite, while reaction of Fe-poor olivine produces substantial amounts of brucite. Thus, the absence of brucite in the products of Hortono230 can be explained by its thermodynamic instability relative to the Fe-rich serpentine plus magnetite mineral assemblage at the experimental conditions (see McCollom et al., 2022).

A more detailed comparison between the experimental observations and thermodynamic equilibrium models is provided in Fig. 6. This figure shows results from Hotono230 projected onto a reaction path model constructed to simulate the progressive reaction of hortonolite at 230 °C (additional outputs of the model are provided in the spreadsheet included as Dataset2). The model predicts the compositions of secondary minerals and of the coexisting fluid as a function of reaction progress (i.e., fraction of olivine reacted), with the assumption that thermodynamic equilibrium is maintained among the secondary mineral products and with the coexisting fluid. The mineral and fluid compositions observed in Hortono230 are projected onto the model results assuming that the hortonolite reacted linearly as a function of time, which is consistent with previous experimental studies of olivine serpentinization (Malvoisin et al., 2012; McCollom et al., 2016).

The comparison in Fig. 6 illustrates that the equilibrium model successfully replicates the mineral and fluid compositions observed in Hortono230. In particular, the model predictions closely replicate the Fe content and Fe^{III}:Fe_{total} ratio of the chrysotile produced in the experiment (Fig. 6c). The model predicts precipitation of ~9 wt% magnetite for the extent of reaction observed in the experiment (Fig. 6a; Dataset2), which is reasonably consistent with the observed amount of 15.3 wt% for the bulk reacted solids. The somewhat lower amount of magnetite predicted by the models reflects a slight overestimate of the total Fe content of serpentine (Fig. 6c), suggesting that some further refinement of the solid solution parameters for serpentine minerals or thermodynamic properties of the endmembers may be needed.

The production of H_2 predicted by the model also agrees closely with experimental observations up to the last measurement, where the models predict a continued linear increase in H_2 generation while the experimental data appear to show a slight decrease in the rate of accumulation over time (Fig. 6b). The reason for this discrepancy is uncertain. A couple of possible explanations are that the decrease in the rate of H_2 accumulation in the latter stage of the experiment represents a change in reaction stoichiometry or a slowing reaction rate; however, results of previous olivine serpentinization studies have indicated that the stoichiometry and rate of the reaction do not change appreciably as the reaction progresses (e.g., Malvoisin et al., 2012; McCollom et al., 2016).

Another possibility is that some of the H_2 generated by serpentinization may have been consumed by reduction of another redox-labile component in the experiment. For instance, reduction of metallic elements during serpentinization can result in precipitation of native metals or metal-alloys such as awaruite (Ni_3Fe;

Table 5
Summary of key experimental results from Hortono230 and related experiments.

Experiment	Duration (h)	Final $pH_{25°C}$	Final $pH_{in\ situ}$	Final H_2 conc. (mmol)	Total H_2 generated (μmol/g)	Mg# Srp	Mg# Brc	Fe^{III}/Fe_{tot}Srp (mol%)	Wt.% Mag	Estimated % reaction*
Hortono230	3525	10.3	7.4	88.5	381	82	n. a.	21	15.3†	55
Oliv230fine#	4293	9.1	7.8	25	47	97	92	–	1.75	25
Oliv230pH‡	2972	12.3	9.3	47	105	93	78	53	1.6	70

* Percent of total primary minerals reacted based on TGA results. Srp = serpentine, Brc = brucite, Mag = magnetite.
† Calculated for bulks solids based on estimate of 80 % dark-grey solids and 20 % light-grey.
# Data for olivine-only experiment at circumneutral pH from McCollom et al. (2016).
‡ Data for olivine-only experiment at strongly alkaline pH from McCollom et al. (2020a). "n.a." = not applicable. "–" = not determined.

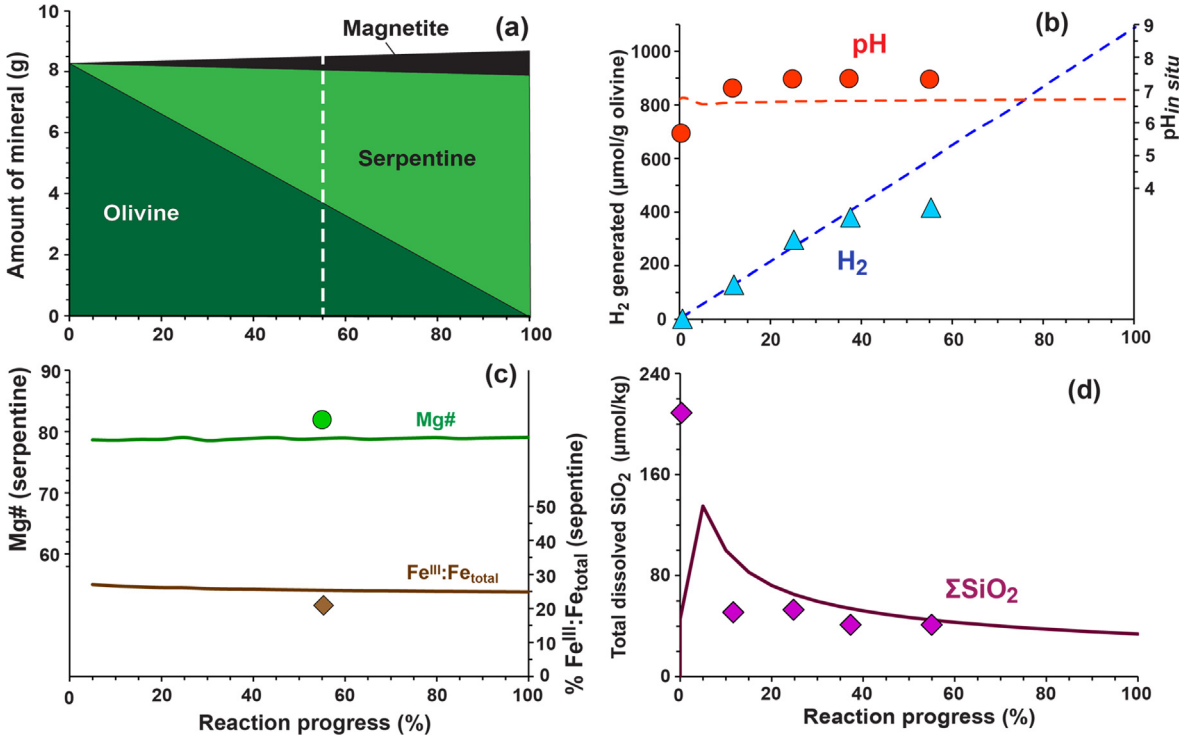

Fig. 6. Results of a reaction path model constructed to simulate reaction of hortonolite at 230 °C, with experimental results from Hortono230 shown for comparison (symbols). (a) Predicted mineral composition as a function of reaction progress. The dashed vertical line indicates the approximate degree of reaction progress in Hortono230. (b) Predicted in situ pH and amount of H_2 generated. (c) Predicted Mg# and Fe^{III}:Fe_{total} ratio (in percent) for serpentine. (d) Concentration of total dissolved ΣSiO_2.

Klein and Bach, 2009; Klein et al., 2009), and reduction of carbon can potentially result in precipitation of solid carbonaceous materials as well (Milesi et al., 2016). With respect to the latter possibility, it may be worth noting that the fluid composition in Hortono230 appears to converge on equilibrium between dissolved CO_2 and a proxy for hydrogenated condensed carbonaceous matter (Fig. 7). Similar trends have been observed in Oliv230fine and other serpentinization experiments as well as in fluids discharged from several natural serpentinites, and suggest that dissolved H_2 and CO_2 levels during serpentinization may be regulated by equilibrium with a solid carbonaceous component under some circumstances (Milesi et al., 2016; Sforna et al., 2018; Ménez et al., 2018). Although native metals or carbonaceous materials were not observed during examination of the Hortono230 products, they may have been present in trace amounts dispersed among the other products that would be difficult to detect without more-detailed analytical methods (e.g., Ellison et al., 2021).

Overall, the good agreement between the experimental and modeling results suggests that thermodynamic equilibrium exerted a predominant influence on the partitioning of Fe among the products of the hortonolite experiment, and on the fraction of Fe^{II} converted to Fe^{III} during the process. Moreover, since the generation of H_2 is dependent on the partitioning of Fe^{III} into secondary minerals (Rxn. 3), the flux of H_2 generated as the reaction proceeds also appears to be regulated largely by thermodynamic equilibrium involving the secondary minerals and components of the fluid. Similarly close agreement with thermodynamic models has been observed in other serpentinization experiments (McCollom et al., 2016, 2020a,b), providing additional support for a prominent role of thermodynamic factors in regulating the partitioning of Fe and H_2 generation during serpentinization. Overall, the results imply that thermodynamic equilibrium among the reaction products may exert a stronger influence on mineral and fluid compositions during serpentinization of natural rocks than other proposed factors such as silica activity, fluid pH, and equilibrium between serpentine and olivine (e.g., Moody, 1976; Evans and Trommsdorf, 1972; Frost and Beard, 2007; Evans, 2008; Syverson et al., 2017).

Although there were additional differences other than olivine composition between Hortono230 and the other serpentinization experiments, these likely played only a very minor role in accounting for differences in Fe partitioning and H_2 generation. The initial fluid for experiments Oliv230fine and Oliv230pH contained dissolved HCO_3^-, but the amounts added were very small and resulted in precipitation of only trace amounts of carbonate minerals, none of which contained Fe: consequently, the addition of HCO_3^- likely had only a very minor influence on the partitioning of Fe and Mg among the product minerals. The addition of NaOH to increase the pH in Oliv230pH resulted in an increase in the partitioning of Fe into serpentine and brucite, which in turn resulted in production of less magnetite and H_2 relative to reaction at less alkaline pH (McCollom et al., 2020a). Because the $pH_{in\ situ}$ was substantially less alkaline in Horotono230 than in Oliv230pH (Fig. 1b), some of the differences between the distribution of Fe contents of mineral products and H_2 production could be driven by the difference in pH. However, any such effect would have been small relative to the much larger variation driven by the differences in Fe content of the reactant olivine.

4.2. Relative reaction rate

As seen in Table 5, the extent of reaction that occurred during Hortono230 is intermediate between that observed for serpentinization of Mg-rich olivine in Oliv230fine and Oliv230pH. A recent experimental study found that the rate of olivine serpentinization is strongly dependent on pH, with more alkaline conditions leading to higher rates of reaction (McCollom et al., 2020a).

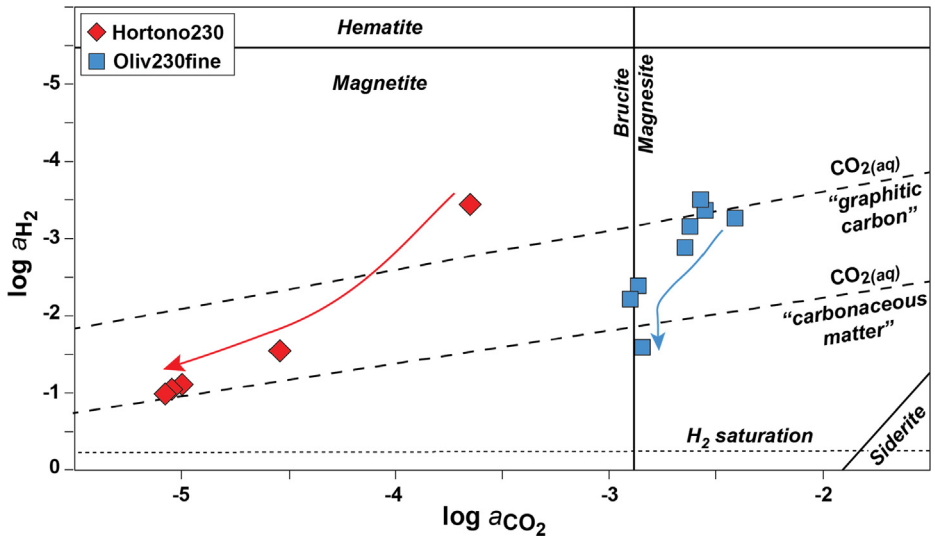

Fig. 7. Fluid compositions during experiments Hortono230 and Oliv230fine projected onto stability diagrams for selected minerals as a function of activities of dissolved CO_2 and H_2. The diagram is constructed for 230 °C and 35 MPa to correspond to conditions used in the experiments. The arrows indicate the trajectory of the fluid composition over time during the experiments. Solid black lines indicate equilibrium between hematite-magnetite, magnetite-siderite, and brucite-magnetite mineral pairs, with individual minerals stable on either side of the lines as noted on the diagram. Dashed lines indicate metastable equilibrium between dissolved CO_2 and graphite or between dissolved CO_2 and anthracene, a proxy for the thermodynamic properties of hydrogenated condensed carbonaceous matter (Milesi et al., 2016). Values for the activities of dissolved CO_2 and H_2 during the experiments are derived from the EQ3 fluid speciation calculations used to determine in situ pH (see methods). The short dashed line reflects saturation of the fluid with respect to dissolved H_2. The brucite-magnesite equilibrium line is calculated for the dissolved Mg concentration in Oliv230fine, where the abundance of dissolved CO_2 is regulated by these minerals; brucite is unstable relative to magnetite in Horoton230, so a similar buffering of a_{CO2} does not occur. Diagram is adapted from Milesi et al., 2016, and details of construction of the diagram are described therein.

The rate of reaction for Hortono230 is compared with results of several other olivine serpentinization experiments performed at 230 °C in Fig. 8, with rates plotted as a function of pH. When pH is taken into account, the reaction rate for Hortono230 appears to be consistent with the trend observed in the other serpentinization experiments, which were performed with Mg-rich SC olivine (Fig. 8). The consistency of the Hortono230 results with the general trend suggests that the higher Fe content of hortonolite did not have a significant impact on the rate of reaction.

The reason for the increased rates of olivine serpentinization with increasing pH remains to be determined. However, dissolution of Mg-rich olivine at alkaline pH appears to proceed through formation of a Si-depleted, Mg-enriched layer on the surface, and the rate-limiting step for dissolution at higher pH is thought to involve hydrolysis and detachment of Mg^{+2} ions from this Si-depleted layer (Pokrovsky and Schott, 2000; Oelkers et al., 2018). If this is the case, then the result from Hortono230 suggests that a similar Mg- and Fe-enriched layer may form at the surface of hortonolite as it dissolves under alkaline conditions, and that Fe^{+2} ions are removed from this layer at a rate comparable to Mg^{+2}.

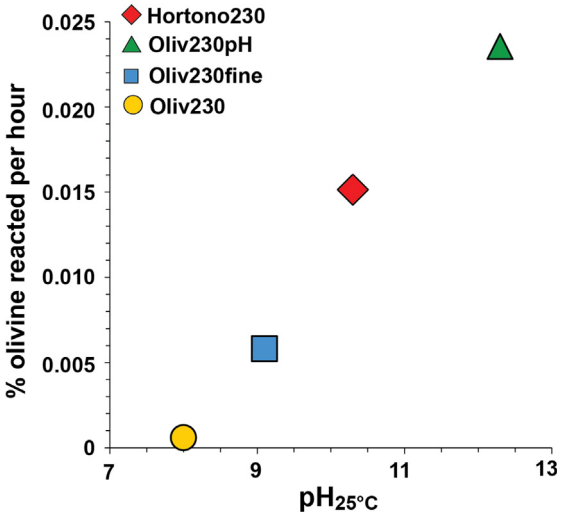

Fig. 8. Rates of reaction for Hortono230 and other olivine serpentinization experiments performed at 230 °C as a function of pH. Data for Oliv230 and Oliv230fine from McCollom et al. (2016) and for Oliv230pH from McCollom et al. (2020a). Except for Hortono230, all the experiments were conducted with Mg# = 90 olivine.

To the extent that the experimental conditions are relevant to the interiors of other planetary bodies, the >50 % reaction progress attained in less than a year for Hortono230 may indicate that serpentinizing systems are relatively short-lived. However, additional factors in natural systems such as restricted water access and larger grain size may reduce reactions rates well below those observed in the experiment. In addition, the rate of serpentinization of olivine appears to decrease substantially at temperatures below 230 °C, at least for Mg-rich olivine compositions (e.g., Wegner and Ernst, 1983; Malvoisin et al., 2012; McCollom et al., 2016). Hence, if the same decrease in rates at lower temperatures applies to more Fe-rich olivine, serpentinization taking place at lower temperatures than in Hortono230 would be expected to be much slower. More data are required to fully understand how serpentinization rates vary as a function of factors such as temperature, pH, and rock composition, but further study could yield insight into the geologic history of other planetary bodies.

4.3. Implications for serpentinization on Mars and icy moons

Serpentinization has been widely invoked as a potential process to support microbial life on Mars and icy moons in the outer solar system (e.g., Schulte et al., 2006; Vance et al., 2007, 2016; Michalski et al., 2013; Glein et al., 2015; Sekine et al., 2015; Greenberger et al., 2015; Onstott et al., 2019; Vance and Melwani Daswani, 2020; Glein and Zolotov, 2020). This proposition is based on studies of analogous environments on Earth, where the H_2 and

CH_4 produced by serpentinization have been found to supply metabolic energy that supports prolific autotrophic microbial communities in a variety of settings (see Schrenk et al., 2013; McCollom and Seewald, 2013; Ménez, 2020; and references therein). If the supply of H_2 is the limiting factor for growth in such environments, the results of this study suggests that serpentinizing systems in extraterrestrial settings may have a substantially greater potential to support microbial activity than in analogous terrestrial environments. For the olivine composition and conditions of the Hortono230 experiment, up to four times as much biomass could potentially be supported based on the amount of H_2 generated.

On Mars, the H_2 generated by serpentinization has also been invoked as a potential contributor to atmospheric greenhouse gases that helped warm the planet's surface in the early solar system (Wordsworth and Pierrehumbert, 2013; Ramirez et al., 2014; Chassefière et al., 2016; Wordsworth, 2016; Wordsworth et al., 2021; Guzewich et al., 2021). If serpentinization was widespread on early Mars, it could have been a major contributor to the H_2 in the atmosphere. The results of Hortono230 suggest that the higher Fe contents of olivine in Martian rocks should enhance their capacity to generate H_2, leading to higher inputs to the atmosphere than would be expected based on terrestrial olivine compositions.

The mineralogical and chemical changes that occur during serpentinization also have substantial effects on the physical properties of the rocks. For example, serpentinization can result in a steep increase in rock magnetization, owing to the formation of magnetite as one of the major reaction products (Toft et al., 1990; Oufi et al., 2002; Klein et al., 2014). Serpentinization also lowers the rock's density by ~20 % while increasing its volume by ~45 %, decreases the rock's tectonic strength, and results in overall oxidation of the bulk rock (Coleman, 1970; Escartin et al., 2001; Guillot et al., 2015; Klein and Le Roux, 2020). One implication of these effects is that serpentinization may make a significant contribution to the magnetic properties of planetary lithospheres. On Mars, for example, serpentinization of rocks within the crust may have been a significant contributor to that planet's magnetic signature and a contributor to the remanent crustal magnetic anomalies observed in the Southern highlands (Quesnel et al., 2009; Chassefière et al., 2013: Lasue et al., 2015).

The results of Hortono230 demonstrate that serpentinization of Fe-rich olivine has the potential to precipitate significantly greater amounts of magnetite than is observed in terrestrial serpentinization systems that are hosted in mantle peridotite (Table 5). If the olivine-rich rocks that undergo serpentinization on other planetary bodies have higher Fe contents than their terrestrial counterparts, they may produce a proportionally stronger magnetic signature. One caveat, however, is that because Fe-brucite is expected to precipitate instead of magnetite during serpentinization of olivine-rich rocks at low temperatures (<100–200 °C, depending on olivine Fe content; Klein et al., 2013; McCollom et al., 2022), the increased magnetization may only be manifested in rocks that undergo serpentinization at relatively high temperatures. In addition, in ultramafic rocks where orthopyroxene contributes significantly to serpentinization, a greater proportion of Fe will partition into serpentine rather than magnetite, reducing the amount of magnetite produced (e.g., Seyfried et al., 2007; Klein et al., 2009, 2013, 2014).

Should serpentinization of olivine on other planetary produce serpentine that is relatively enriched in Fe, the results of VNIR and Raman analyses suggest that the higher Fe contents should be detectable by remote methods. In particular, higher Fe contents for serpentine may result in a shift to lower wavelengths in VNIR spectra (Fig. 5) and a lower Raman shift in Raman spectra (Supplemental Fig. S3). However, additional analyses for a wider range of serpentine compositions will be needed to confirm and calibrate these trends before they can be used to confidently assign specific compositions to serpentine minerals on Mars or other planetary bodies.

5. Conclusions

Experimental serpentinization of the Fe-rich hortonolite at 230 °C resulted in formation of chrysotile, magnetite, and H_2. Compared to reaction of Mg-rich olivine under similar conditions, the chrysotile produced from hortonolite had higher Fe contents, and significantly greater amounts of magnetite and H_2 were generated. The abundances and composition of the reaction products are consistent with predictions of thermodynamic models, providing additional support for the proposition that thermodynamic equilibrium among the reaction products exerts a predominant influence on regulating the outcome of serpentinization reactions. The results suggest that serpentinization of olivine-rich rocks on other planetary bodies may have a greater capacity to support autotrophic biological communities, enhance atmospheric greenhouse warming, and generate stronger magnetic signatures than equivalent terrestrial serpentinites. In addition, the fluids produced were alkaline, with very low concentrations of Fe, Mg, and SiO_2, which may have implications for interpreting the role of serpentinization in regulating the chemistry of fluids on icy moons and Mars.

Data availability

All data are included as tables in the paper or as supplemental files accompanying the paper.

Declaration of Competing Interest

The authors declare that they have no known competing financial interests or personal relationships that could have appeared to influence the work reported in this paper.

Acknowledgments

This research was supported by the NASA Solar Systems Working program through grant NNX16AL74G. The IRM is a US National Multi-user Facility supported by the Instruments and Facilities Program of the NSF Division of Earth Science. This is IRM contribution # 2108. We are grateful to Dr. Marian Lupulescu from the New York State Museum for providing the hortonolite dunite used in this study.

Appendix A. Supplementary material

Supplementary material to this article can be found online at https://doi.org/10.1016/j.gca.2022.08.025.

References

Agee, C.B., 1993. High-pressure melting of carbonaceous chondrite. J. Geophys. Res. – Planets 98, 5419–5426.
Amador, E.S., Bandfield, J.L., Thomas, N.H., 2018. A search for minerals associated with serpentinization across Mars using CRISM spectral data. Icarus 311, 113–134.
Andreani, M., Daniel, I., Pollet-Villard, M., 2013. Aluminum speeds up the hydrothermal alteration of olivine. Amer. Mineral. 98, 1738–1744.
Berndt, M.E., Allen, D.E., Seyfried Jr., W.E., 1996. Reduction of CO_2 during serpentinization of olivine at 300°C and 500 bar. Geology 24, 351–354.
Bethke, C.M., 2008. Geochemical and Biogeochemical Reaction Modeling. Cambridge University Press.
Bultel, B., Quantin-Nataf, C., Andréani, M., Clénet, H., Lozac'h, L., 2015. Deep alteration between Hellas and Isidis Basins. Icarus 260, 141–160.
Cannat, M., Fontaine, F., Escartin, J., 2010. Serpentinization and associated hydrogen and methane fluxes at slow spreading ridges. In: Rona, P.A., Devey, C.W., Dement, J., Murton, B.J. (Eds.), *Diversity of Hydrothermal Systems on Slow*

Spreading Ridges. Geophysical Monograph Series, vol. 188. American Geophysical Union, pp. 241–264.
Chassefière, E., Langlais, B., Quesnel, Y., Leblanc, F., 2013. The fate of early Mars' lost water: The role of serpentinization. J. Geophys. Res. – Planets 118, 1123–1134.
Chassefière, E., Lasue, J., Langlais, B., Quesnel, Y., 2016. Early Mars serpentinization-derived CH_4 reservoirs, H_2-induced warming and paleopressure evolution. Meteor. Planet. Sci. 51, 2234–2245.
Coleman, R.G., 1977. Ophiolites: ancient oceanic lithosphere? Springer Verlag, Berlin, p. 229.
Dyar, M.D., Agresti, D.G., Schaefer, M.W., Grant, C.A., Sklute, E.C., 2006. Mossbauer spectroscopy of earth and planetary minerals. Ann. Rev. Earth Planet. Sci. 34, 83–125.
Ehlmann, B.L., Mustard, J.F., Murchie, S.L., 2010. Geologic setting of serpentine deposits on Mars. Geophys. Res. Lett. 37, L06201.
Ellison, E.T., Templeton, A.S., Zeigler, S.D., Mayhew, L.E., Kelemen, P.B., Matter, J.M., the Oman Science Drilling Party, 2021. Low-temperature hydrogen formation during aqueous alteration of serpentinized peridotite in the Samail Ophiolite. J. Geophys. Res. – Solid Earth 126. e2021JB021981.
Evans, B.W., 2008. Control of the products of serpentinization by the $Fe^{+2}Mg_{-1}$ exchange potential of olivine and orthopyroxene. J. Petrol. 49, 1873–1887.
Evans, B.W., Trommsdorf, V., 1972. Die einfluss des eisens auf die hydratisierung von duniten. Schweiz. Min. Pet. Mitt. 52, 251–256.
Evans, B.W., Hattori, K., Baronnet, A., 2013. Serpentinite: What, why, where? Elements 9, 99–106.
Foustoukos, D.I., Savov, I.P., Janecky, D.R., 2008. Chemical and isotopic constraints on water/rock interactions at the Lost City hydrothermal field, 30°N Mid-Atlantic Ridge. Geochim. Cosmochim. Acta 72, 5457–5474.
Frost, B.R., Beard, J.S., 2007. On silica activity and serpentinization. J. Petrol. 48, 1351–1368.
Glein, C.R., Zolotov, M.Y., 2020. Hydrogen, hydrocarbons, and habitability across the universe. Elements 16, 47–52.
Glein, C.R., Baross, J.A., Waite Jr., J.H., 2015. The pH of Enceladus' ocean. Geochim. Cosmochim. Acta 162, 202–219.
Greenberger, R.N., Mustard, J.F., Cloutis, E.A., Pratt, L.M., Sauer, P.E., Mann, P., Turner, K., Dyar, M.D., Bish, D.L., 2015. Serpentinization, iron oxidation, and aqueous conditions in an ophiolite: Implications for hydrogen production and habitability on Mars. Earth Planet. Sci. Lett. 416, 21–34.
Grozeva, N.G., Klein, F., Seewald, J.S., Sylva, S.P., 2017. Experimental study of carbonate formation in oceanic peridotites. Geochim. Cosmochim. Acta 199, 264–286.
Guillot, S., Schwartz, S., Reynard, B., Agard, P., Prigent, C., 2015. Tectonic significance of serpentinites. Tectonophysics 646, 1–19.
Guzewich, S.D., Way, M.J., Aleinov, I., Wolf, E.T., Del Genio, A., Wordsworth, R., Tsigaridis, K., 2021. 3D simulations of the early martian hydrological cycle mediated by a H_2-CO_2 greenhouse. J. Geophys. Res. - Planets 126. e2021JE006825.
Hanowski, N.P., Brearley, A.J., 2001. Aqueous alteration of chondrules in the CM carbonaceous chondrite, Allan Hills 81002; Implications for parent body alteration. Geochim. Cosmochim. Acta 65, 495–518.
Hicks, L.J., Bridges, J.C., Gurman, S.J., 2014. Ferric saponite and serpentine in the nakhlite martian meteorites. Geochim. Cosmochim. Acta 136, 194–210.
Hsu, H.-W., Postberg, F., Sekine, Y., Shibuya, T., Kempf, S., Horányi, M., Juhász, A., Altobellu, N., Suzuki, K., Masaki, Y., Kuwatani, T., Tachibana, S., Sirono, S., Moragas-Klostermeyer, G., Srama, R., 2015. Ongoing hydrothermal activities within Enceladus. Nature 519, 207–210.
Jones, L.C., Rosenbauer, R., Goldsmith, J.I., Oze, C., 2010. Carbonate control of H_2 and CH_4 production in serpentinization systems at elevated P-Ts. Geophys. Res. Lett. 37, L14306.
Keller, L.P., Buseck, P.R., 1990. Matrix mineralogy of the Lance CO3 carbonaceous chondrite: A transmission electron microscope study. Geochim. Cosmochim. Acta 54, 1155–1163.
Khan, A., Connolly, J.A.D., 2008. Constraining the composition and thermal state of Mars from inversion of geophysical data. J. Geophys. Res. 113, E07003.
Klein, F., Bach, W., 2009. Fe-Ni-Co-O-S phase relations in peridotite seawater interactions. J. Petrol. 50, 37–59.
Klein, F., Le Roux, V., 2020. Quantifying the volume increase and chemical exchange during serpentinization. Geology 48, 552–556.
Klein, F., Bach, W., Jöns, N., McCollom, T.M., Moskovitz, B., Berquo, T., 2009. Iron partitioning and hydrogen generation during serpentinization of abyssal peridotites from 15°N on the Mid-Atlantic Ridge. Geochim. Cosmochim. Acta 73, 6868–6893.
Klein, F., Bach, W., McCollom, T.M., 2013. Compositional controls on hydrogen generation during serpentinization of ultramafic rocks. Lithos 99, 377–386.
Klein, F., Bach, W., Humphris, S.E., Kahl, W.-A., Jöns, N., Moskowitz, B., Berquó, T.S., 2014. Magnetite in seafloor serpentinite - Some like it hot. Geology 42, 135–138.
Klein, F., Grozeva, N.G., Seewald, J.S., McCollom, T.M., Humphris, S.E., Moskovitz, B., Berquo, T.S., Kahl, W.-A., 2015. Experimental constraints on fluid-rock interactions during incipient serpentization of harzburgite. Am. Mineral. 100, 991–1002.
Klein, F., Grozeva, N.G., Seewald, J.S., 2019. Abiotic methane synthesis and serpentinization in olivine-hosted fluid inclussions. Proc. Nat. Acad. Sci. USA 116, 17666–17672.
Koeppen, W.C., Hamilton, V.E., 2008. Global distribution, composition, and abundance of olivine on the surface of Mars from thermal infrared data. J. Geophys. Res. 113, E05001.
Kokaly, R.F., Clark, R.N., Swayze, G.A., Livo, K.E., Hoefen, T.M., Pearson, N.C., Wise, R. A., Benzel, W.M., Lowers, H.A., Driscoll, R.L., Klein, A.J., 2017 USGS Spectral Library Version 7: U.S. Geological Survey Data Series 1035, 61 p., doi:10.3133/ds1035.
Lasue, J., Quesnel, Y., Langlais, B., Chassefière, E., 2015. Methane storage capacity of the early martian cryosphere. Icarus 260, 205–214.
Malvoisin, B., Brunet, F., Carlut, J., Rouméjon, S., Cannat, M., 2012. Serpentinization of oceanic peridotites: 1: A high-sensitivity method to monitor magnetite production in hydrothermal experiments. J. Geophys. Res. 117, B01104.
Marcaillou, C., Muñoz, M., Vidal, O., Parra, T., Harfouche, M., 2011. Mineralogical evidence for H_2 degassing during serpentinization at 300 °C/300 bar. Earth Planet. Sci. Lett. 303, 281–290.
Martin, B., Fyfe, W.S., 1970. Some experimental and theoretical observations on the kinetic of hydration reactions with particular reference to serpentinization. Chem. Geol. 6, 185–202.
Mayhew, L.E., Ellison, E.T., 2020. A synthesis and meta-analysis of the Fe chemistry of serpentinites and serpentine minerals. Phil. Trans. Roy. Soc. A. 378, 20180420.
McCollom, T.M., 2016. Abiotic methane formation during experimental serpentinization of olivine. Proc. Nat. Acad. Sci. USA 113, 13965–13970.
McCollom, T.M., Bach, W., 2009. Thermodynamic constraints on hydrogen generation during serpentinization of ultramafic rocks. Geochim. Cosmochim. Acta 73, 856–875.
McCollom, T.M., Klein, F., Ramba, M., 2022. Hydrogen Generation from Serpentinization of Iron-rich Olivine on Mars, Icy Moons, and Other Planetary Bodies. Icarus 372, 114754.
McCollom, T.M., Seewald, J.S., 2001. A reassessment of the potential for reduction of dissolved CO_2 to hydrocarbons during serpentinization of olivine. Geochim. Cosmochim. Acta 65, 3769–3778.
McCollom, T.M., Klein, F., Solheid, P., Moskowitz, B., 2020a. The effect of pH on rates of reaction and hydrogen generation during serpentinization. Phil. Trans. Roy. Soc. A. 378, 20180428.
McCollom, T.M., Klein, F., Moskowitz, B., Berquó, T.S., Bach, W., Templeton, A.S., 2020b. Hydrogen generation and iron partitioning during experimental serpentinization of an olivine–pyroxene mixture. Geochim. Cosmochim. Acta 282, 55–75.
McCollom, T.M., Seewald, J.S., 2007. Abiotic synthesis of organic compounds in deep-sea hydrothermal environments. Chem. Rev. 107, 382–401.
McCollom, T.M., Seewald, J.S., 2013. Serpentinites, hydrogen, and life. Elements 9, 129–134.
McCollom, T.M., Klein, F., Robbins, M., Moskowitz, B., Berquó, T.S., Jöns, N., Bach, W., Templeton, A., 2016. Temperature trends for reaction rates, hydrogen generation, and partitioning of iron during experimental serpentinization of olivine. Geochim. Cosmochim. Acta 181, 175–200.
McCollom T.M., 2013. Laboratory simulations of abiotic hydrocarbon formation in Earth's deep subsurface. In: Hazen, R.M., Jones, A.P., Baross, J. (Eds.), Carbon in Earth. *Rev. Mineral. Geochem.* vol. 75, pp. 467–494.
McSween Jr., H.Y., 1977. On the nature and origin of isolated olivine grains in carbonaceous chondrites. Geochim. Cosmochim. Acta 41, 411–418.
Ménez, B., 2020. Abiotic hydrogen and methane: fuels for life. Elements 16, 39–46.
Ménez, B., Pasini, V., Guyot, F., Benzerara, K., Bernard, S., Brunelli, D., 2018. Mineralizations and transition metal mobility driven by organic carbon during low-temperature serpentinization. Lithos 323, 262–276.
Merdith, A.S., Garcia del Real, P., Daniel, I., Andreani, M., Wright, N.M., Coltice, N., 2020. Pulsated global hydrogen and methane flux at mid-ocean ridges driven by Pangea breakup. Geochem. Geophys. Geosyst. 21. e2019GC008869.
Michalski, J.R., Cuadros, J., Niles, P.B., Parnell, J., Rogers, A.D., Wright, S.P., 2013. Groundwater activity on Mars and implications for a deep biosphere. Nat. Geosci. 6, 133–138.
Milesi, V., McCollom, T., Guyot, F., 2016. Thermodynamic constraints on the formation of condensed carbon from serpentinization fluids. Geochim. Cosmochim. Acta 189, 391–403.
Milliken, R.E., Rivkin, A.S., 2009. Brucite and carbonate assemblages from altered olivine-rich materials on Ceres. Nat. Geosci. 2, 258–261.
Moody, J.B., 1976. An experimental study on the serpentinization of iron-bearing olivines. Can. Mineral. 14, 462–478.
Oelkers, E.H., Declerq, J., Saldi, G.D., Gislason, S.R., Schott, J., 2018. Olivine dissolution rates: A critical review. Chem. Geol. 500, 1–19.
Ogasawara, Y., Okamoto, A., Hirano, N., Tsuchiya, N., 2013. Coupled reactions and silica diffusion during serpentinization. Geochim. Cosmochim. Acta 119, 212–230.
Okamoto, A., Ogasawara, Y., Ogawa, Y., Tsuchiya, N., 2011. Progress of hydration reactions in olivine-H_2O and orthopyroxenite-H_2O systems at 250 °C and vapor-saturated pressure. Chem. Geol. 289, 245–255.
Onstott, T.C., Ehlmann, B.L., Sapers, H., Coleman, M., Ivarsson, M., Marlow, J.J., Neubeck, A., Niles, P., 2019. Paleo-rock-hosted life in Earth and the search for life on Mars: A review and strategy for exploration. Astrobiology 19, 1–33.
Oufi, O., Cannat, M., Horen, H., 2002. Magnetic properties of variably serpentinized abyssal peridotite. J. Geophys. Res. 107, B5.
Papike, J.J., Karner, J.M., Shearer, C.K., Burger, P.V., 2009. Silicate mineralogy of martian meteorites. Geochim. Cosmochim. Acta 73, 7443–7485.
Pokrovsky, O.S., Schott, J., 2000. Kinetics and mechanism of forsterite dissolution at 25°C and pH from 1 to 12. Geochim. Cosmochim. Acta 64, 3313–3325.
Proskurowksi, G., Lilley, M.D., Kelley, D.S., Olson, E.J., 2006. Low temperature volatile production at the Lost City Hydrothermal Field, evidence from a hydrogen stable isotope geothermometer. Chem. Geol. 229, 331–343.

Proskurowksi, G., Lilley, M.D., Seewald, J.S., Früh-Green, G.L., Olson, E.J., Lupton, J.E., Sylva, S.P., Kelley, D.S., 2008. Abiogenic hydrocarbon production at Lost City Hydrothermal Field. Science 319, 604–607.

Quesnel, Y., Sotin, C., Langlais, B., Costin, S., Mandea, M., Gottschalk, M., Dyment, J., 2009. Serpentinization of the martian crust during the Noachian. Earth Planet. Sci. Lett. 277, 184–193.

Ramirez, R.M., Kopparapu, R., Zugger, M.E., Robinson, T.D., Freedman, R., Kasting, J. F., 2014. Warming early Mars with CO_2 and H_2. Nature Geosci. 7, 59–63.

Rubin, A.E., 1990. Kamacite and olivine in ordinary chondrites: Intergroup and intragroup relationships. Geochim. Cosmochim. Acta 54, 1217–1232.

Schrenk, M.O., Brazelton, W.J., Lang, S.Q., 2013. Serpentinization, carbon, and deep life. In: Hazen, R.M., Jones, A.P., Baross, J. (Eds.), Carbon in Earth. *Rev. Mineral. Geochem.* vol. 75, pp. 575–606.

Schulte, M., Blake, D., Hoehler, T., McCollom, T.M., 2006. Serpentinization and its implications for life on the early Earth and Mars. Astrobiology 6, 364–376.

Sekine, Y., Shibuya, T., Postberg, F., Hsu, H.-W., Suzuki, K., Masaki, Y., Kuwatani, T., Mori, M., Hong, P.K., Yoshizaki, M., Tachibana, S., Sirono, S., 2015. High-temperature water-rock interactions and hydrothermal environments in the chondrite-like core of Enceladus. Nat. Comm. 6, 8604.

Seyfried Jr., W.E., Foustoukos, D.I., Fu, Q., 2007. Redox evolution and mass transfer during serpentinization: An experimental and theoretical study at 200 °C, 500 bar with implications for ultramafic-hosted hydrothermal systems at Mid-Ocean Ridges. Geochim. Cosmochim. Acta 71, 3872–3886.

Seyfried Jr., W.E., Janecky, D.R., Berndt, M.E., 1987. Rocking autoclaves for hydrothermal experiments, II. The flexible reaction-cell system. In: Ulmer, G. C., Barnes, H.L. (Eds.), Hydrothermal Experimental Techniques. John Wiley and Sons, pp. 216–239.

Sforna, M.C., Brunelli, D., Pisapia, C., Pasini, V., Malferrari, D., Ménez, B., 2018. Abiotic formation of condensed carbonaceous matter in the hydrating crust. Nat. Comm. 9, 5049.

Shibuya, T., Yoshizaki, M., Sato, M., Shimizu, K., Nakamura, K., Omori, S., Suzuki, K., Takai, K., Tsunakawa, H., Maruyama, S., 2015. Hydrogen-rich hydrothermal environments in the Hadean ocean inferred from serpentinization of komatiites at 300 °C and 500 bar. Prog. Earth Planet. Sci. 2, 46.

Syverson, D.D., Tutolo, B.M., Borrok, D.M., Seyfried Jr., W.E., 2017. Serpentinization of olivine at 300 °C and 500 bars: An experimental study examining the role of silica on the reaction path and oxidation state of iron. Chem. Geol. 475, 122–134.

Szitkar, F., Tivey, M.A., Kelley, D.S., Karson, J.A., Früh-Green, G.L., Denny, A.R., 2017. Magnetic exploration of a low-temperature ultramafic-hosted hydrothermal site (Lost City, 30°N, MAR). Earth Planet. Sci. Lett. 461, 40–45.

Templeton, A.S., Ellison, E.T., Glombitza, C., Morono, Y., Rempfert, K.R., Hoehler, T. M., Zeigler, S.D., Kraus, E.A., Spear, J.R., Nothaft, D.B., Fones, E.M., Boyd, E.S., Munro-Ehrlich, M., Mayhew, L.E., Cardace, D., Matter, J.M., Kelemen, P.B., the Oman Science Drilling Party, 2021. Accessing the subsurface biosphere within rocks undergoing active low-temperature serpentinization in the Samail Ophiolite (Oman Drilling Project). J. Geophys. Res. – Biogeosciences 126. e2021JG006315.

Toft, P.B., Arkani-Hamed, J., Haggert, S.E., 1990. The effects of serpentinization on density and magnetic susceptibility: a petrophysical model. Phys. Earth Planet. Interiors 65, 137–157.

Tutolo, B.M., Evans, B.W., Kuehner, S.M., 2019. Serpentine-hisingerite solid solution in altered ferroan peridotite and olivine gabbro. Minerals 9, 47.

Vance, S., Harnmeijer, J., Kimura, J., Hussmann, H., Demartin, B., Brown, M.J., 2007. Hydrothermal systems in small ocean planets. Astrobiology 7, 987–1005.

Vance, S., Hand, K.P., Pappalardo, R.T., 2016. Geophysical controls of chemical disequilibria in Europa. Geophys. Res. Lett. 43, 4871–4879.

Vance, S.D., Melwani Daswani, M., 2020. Serpentinite and the search for life beyond Earth. Phil. Trans. R. Soc. A 378, 20180421.

Velbel, M.A., 2009. Dissolution of olivine during natural weathering. Geochim. Cosmochim. Acta 73, 6098–6113.

Velbel, M.A., Tonui, E.K., Zolensky, M.E., 2012. Replacement of olivine by serpentine in the carbonaceous chondrite Nogoya (CM2). Geochim. Cosmochim. Acta 87, 117–135.

Velbel, M.A., Tonui, E.K., Zolensky, M.E., 2015. Replacement of olivine by serpentine in the Queen Alexandra Range 93005 carbonaceous chondrite (CM2): Reactant-product relations, and isovolumetric constraints on reaction stoichiometry and elemental mobility during aqueous alteration. Geochim. Cosmochim. Acta 148, 402–425.

Wada, I., Wang, K., He, J., Hyndman, R.D., 2008. Weakening of the subduction interface and its effects on surface heat flow, slab dehydration, and mantle wedge serpentinization. J. Geophys. Res. 113, B04402.

Waite, J.H., Glein, C.R., Perryman, R.S., Teolis, B.D., Magee, B.A., Miller, G., Grimes, J., Perry, M.E., Miller, K.E., Bouquet, A., Lunine, J.I., Brockwell, T., Bolton, S.J., 2017. Cassini finds molecular hydrogen in the Enceladus plume: Evidence for hydrothermal processes. Science 356, 155–159.

Wegner, W.W., Ernst, W.G., 1983. Experimentally determined hydration and dehydration reaction rates in the system MgO-SiO_2-H_2O. Am. J. Sci. 283-A, 151–180.

Wolery, T.J., Jarek, R.L., 2003. *Software user's manual: EQ3/6, Version 8.0.* Lawrence Livermore National Laboratory, Livermore, Calif.

Wordsworth, R., 2016. The climate of early Mars. Annu. Rev. Earth Planet. Sci. 44, 381–408.

Wordsworth, R., Pierrehumbert, R., 2013. Hydrogen-nitrogen greenhouse warming in Earth's early atmosphere. Science 339, 64–67.

Wordsworth, R., Knoll, A.H., Hurowitz, J., Baum, M., Ehlmann, B.L., Head, J.W., Steakley, K., 2021. A coupled model of episodic warming, oxidation and geochemical transitions on early Mars. Nat. Geosci. 14, 127–132.

Yoshizaki, T., McDonough, W.F., 2020. The composition of Mars. Geochim. Cosmochim. Acta 273, 137–162.